JURNAL MATEMATIKA, STATISTIKA DAN KOMPUTASI e-ISSN: 2614-8811
Published by Departement of Mathematics, Hasanuddin University, Indonesia
https://journal.unhas.ac.id/index.php/jmsk/index
Vol. 22, No. 2, January 2026, pp. 256-275
DOI: 10.20956/j.v22i2.47341

Nonlinear Robust Sliding Mode Control for Measles with Parameter Uncertainties

Sailah Ar Rizka[1*], Regina Wahyudyah Sonata Ayu[2], Hanna Hilyati Aulia[3], M. Ziaul Arif[4], Millatuz Zahroh[5]
[1,4,5]Department of Mathematics, Universitas Jember, Jember, Indonesia
[2]Department of Mathematics, Universitas Palangka Raya, Palangka Raya, Indonesia
[3]Department of Sharia Economics, IAIN Metro, Metro, Indonesia
***Email**: [1]sailah.fmipa@unej.ac.id, [2]reginawsayu@mipa.upr.ac.id, [3]hannahilyatiaulia@metrouniv.ac.id, [4]ziaul.fmipa@unej.ac.id, [5]millatuz@unej.ac.id*
**Corresponding author*

Abstract

Measles is a highly contagious viral disease that persists as a global threat following its resurgence in 2018–2019. The SVEIR epidemic model is considered to represent the dynamics of measles. Various factors affecting the spread of measles result in uncertainties and imprecision in the modelling of measles, thereby a robust control strategy is required to eradicate the disease. The aim of the study is to design a nonlinear robust sliding mode control to drive the number of individuals exposed to or infected with measles to zero through a targetted tracking scheme, despite uncertainties in measles dynamics. This is achieved by administering treatments to exposed and infected individuals while maintaining the existing levels of vaccination. The proposed control strategies have been proven to achieve the tracking objective analytically by employing Lyapunov's stability theorem and Barbalat's Lemma. Employing an adaptive switching gain that is updated online during the design process eliminates the necessity of prior information on the bounds of model uncertainties. Numerical simulations of different cases involving parameter uncertainty and diminishing rates were carried out to evaluate control performance. Using a saturation function and a tangent hyperbolic function instead of a sign function in the controllers and adjusting the rate of switching gain updating can reduce chattering incidents arising from the implementation of sliding mode control. Within the nine cases of parameter uncertainties considered, the robust sliding mode control strategy is effective in eradicating the disease, with average reductions in the number of exposed and infected individuals of 80.82–81.57% and 81.01–84.18%, respectively.

Keywords: *adaptive gain; epidemic model; measles; nonlinear robust control; parameter uncertainties; sliding mode control*.

1. INTRODUCTION AND PRELIMINARIES

1.1 Introduction

Measles is an airborne, highly infectious disease affecting people of all ages, caused by a virus classified as a Morbillivirus in the Paramyxoviridae family. The rapid spread of measles is evident from its high basic reproduction number, which indicates that each infected person can infect 12-18 other susceptible individuals [6]. It is transmitted in the four days before symptoms such as rash arise, enabling it to silently spread before the disease is diagnosed. After declining since 1997, a resurgence of measles was observed in 2018–2019, following a decrease in vaccination coverage due to the COVID-19 pandemic [18]. Measles persists as a global threat, with 359,521 cases reported worldwide in 2024 [18]. More than 40% of the reported cases were children under 5 years old in 53 countries in Europe and Central Asia, with more than half of them requiring hospitalization. Measles can cause severe complications, including pneumonia, encephalitis, diarrhea, and dehydration, which might lead to death. In spite of the measles vaccine's availability, an estimated 107,500 measles-related deaths occurred globally in 2023, primarily among children under 5 years old, including both vaccinated and unvaccinated individuals [17]. Furthermore, measles can cause long-term health issues for survivors, with children being at the greatest risk of serious complications. In order to properly contain the regular spread of measles across continents, a better understanding of its transmission dynamics is required.

Mathematical modelling provides a tool to analyze the transmission dynamics of a disease and, hence, could help public health stakeholders to develop the right control strategy against the various factors affecting disease mitigation. A measles model of SEIR and optimal control strategies is proposed by [5], with the employment of prevention, vaccination, and treatment. Optimal control strategies that incorporate vaccination and treatments into a developed SVEITR measles model are also proposed by [10], who consider different ranges of applicable control values, and by [1], who employ NSFD (Non-Standard Finite Difference) to estimate the solutions. Di Giamberardino & Iacoviello [8] expands the classical SEIR model by adding immunosuppressed and infected with comorbidities compartments and also propose optimal control strategies through vaccination, informative campaigns, and treatments. A more realistic SEIR model with a fractional-order differential operator representing the effect of vaccination and its corresponding optimal control strategies of medical (vaccination) and non-medical measures (quarantine and contact tracing) is constructed in [7], showing that vaccination has a significant impact in mitigating measles.

The spread of measles is affected by various factors, including vaccination coverage, immunity gaps, population movement, environmental conditions, the availability of healthcare, and even socioeconomic and political factors. This leads to some uncertainty and imprecision in the modeling of measles dynamics. However, the proposed models, together with their optimal control strategies, which were already mentioned above, assumed the certainty and well-known values of the model parameters. It implies that further control strategies that are robust to uncertainties affecting the disease's mitigation should be developed. In order to address this situation, a robust and adaptive control technique is employed.

Earlier studies have employed robust control strategies to combat the spread of disease despite the inaccuracies and uncertainties of its transmission dynamics, one such strategy being sliding mode control. Sliding mode control is one of the robust control strategies that excels because it is less sensitive to parameter uncertainties and disturbances of the system, thereby relaxing the necessity of exact modelling. The simple design process of sliding mode controls makes them applicable to epidemic models. In [4], sliding mode control with state and parameter estimation employing LSTM (Long Short-Term Memory) algorithm and extended Kalman filter has been implemented into a COVID-19 dynamic of six states and three control inputs. Sliding mode control

employing adaptive sliding gain in the design process has been implemented to mitigate infections in the general SEIR model [9], the influenza model [14], the cholera model [2], and the tuberculosis model [3].

In this study, a robust sliding mode control is designed to eradicate measles disease through tracking a desired reference signal scheme that has not been proposed before, to the utmost of the author's knowledge. This is achieved by administering treatments to individuals exposed to or infected with measles, despite parameter uncertainties in the transmission dynamics. The necessity of prior information of the bounds of model uncertainties is eliminated by employing an adaptive switching gain that is updated online during the design process. The stability of the closed-loop system and the corresponding tracking error are derived from the Lyapunov stability theorem and Barbalat's Lemma.

2. METHOD

This study uses a quantitative methodology based on mathematical theory, utilising numerical simulations to evaluate the results. The study is conducted following the flow diagram of research methodology given in Figure 2.1. The study begins with literature reviews on modelling the spread of measles, followed by determining the control interventions to mitigate measles, and then designing the nonlinear robust sliding mode control. Once the sliding mode controller has been obtained, the stability of the closed-loop system (tracking scheme) is proven using the Lyapunov stability theorem and Barbalat's Lemma. The performance of the controller is also evaluated through simulation. This involves numerous scenarios of parameter uncertainties and tracking error convergence rates. Finally, the simulation results are analysed to evaluate the effectiveness of the control strategy in eradicating measles outbreaks despite the existence of parameter uncertainties.

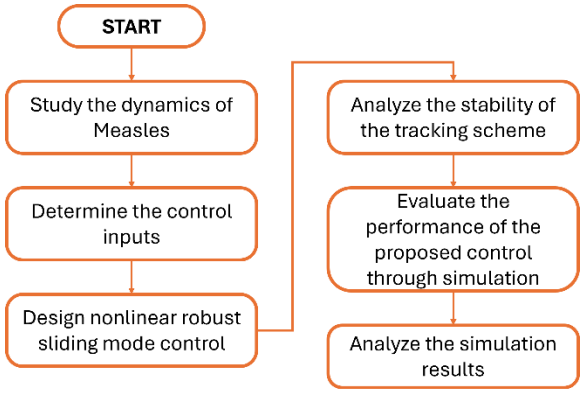

Figure 2.1. Flow diagram of the research methodology.

3. MAIN RESULTS

3.1. Measles Model with Controls

The dynamics of measles outbreaks under study are taken from [16], which consist of five compartments: susceptible (S), vaccinated (V), exposed (E), infected (I), and recovered (R) individuals. Three control inputs embedded into the model [16] are vaccination, treatments for exposed and infected individuals. As the additional vaccination intervention has an insignificant effect on mitigating measles in [16], the control efforts considered here only involve treatments for exposed and infected individuals. Hence, the dynamics of measles outbreaks with two controls are given by

$$\begin{aligned}
\dot{S}(t) &= \Lambda(1-q) + \gamma V(t) - \beta S(t)\big(E(t)+I(t)\big) - (u_1+\mu)S(t)\\
\dot{V}(t) &= \Lambda q + u_1 S(t) - (\gamma+\omega+\mu)V(t)\\
\dot{E}(t) &= \beta S(t)\big(E(t)+I(t)\big) - (\kappa_1(t)+\alpha+u_2+\mu)E(t)\\
\dot{I}(t) &= \alpha E(t) - (\kappa_2(t)+\delta+u_3+\mu)I(t)\\
\dot{R}(t) &= (\kappa_1(t)+u_2)E(t) + \omega V(t) + (\kappa_2(t)+u_3)I(t) - \mu R(t)
\end{aligned} \tag{3.1}$$

The descriptions and values of the model parameters, are given in Table 3.1. Individuals are recruited into the population at a rate of Λ, with a proportion q representing newborns who receive vaccinations, while the remainder remain in the S compartment. The parameter μ denotes the rate of natural death, while δ denotes the rate of disease-related death due to measles. The infection rate for susceptible individuals is proportional to the number of exposed (E) and infected (I) individuals, with a transmission rate of β. Vaccinated (V) individuals return to the S compartment as the vaccine's efficacy reduces at a rate of γ, and they recover at a rate of ω. The parameters u_1 is the vaccination rate for susceptible (S) individuals, while u_2 and u_3 are the recovery rates for exposed (E) and infected (I) individuals, respectively. Furthermore, exposed (E) individuals progress to the infected (I) compartment at the rate α.

Table 3.1. The model parameters' descriptions and values [16]

Symbol	Description	Value
Λ	Recruitment rate	10
β	Transmission rate	0.09091
μ	Natural death rate	0.00875
γ	Declining rate of measles vaccine efficacy	0.167
q	Proportion of newborns receiving vaccination	0.5
α	Progression rate from exposed (E) to infected (I) compartments	0.125
ω	Recovery rate for vaccinated (V) individuals	0.8
δ	Death rate due to measles	0.03
u_1	Vaccination rate against measles	0.2
u_2	Recovery rate for exposed (E) individuals	0.1
u_3	Recovery rate for infected (I) individuals	0.14286

The controls, κ_1 and κ_2, respectively represent the proportion of exposed (E) and infected (I) individuals receiving treatments. The values of controls are constrained to $0 \le \kappa_1, \kappa_2 \le 0.9$ meaning that no interventions is implemented if the value is zero and 0.9 of the respective individuals receive treatment if the values is 0.9.

By using the Next Generation Matrix operator [15,16], the basic reproduction number, R_0, for system (3.1) when the controls are present, is given by

$$R_0(\kappa_1,\kappa_2) = \frac{\beta S_0}{\Phi_1+\kappa_1}\left(1+\frac{\alpha}{\Phi_2+\kappa_2}\right), \tag{3.2}$$

where

$$S_0 = \frac{\Lambda(1-q)(\mu+\omega)+\Lambda\gamma}{(u_1+\mu)(\mu+\omega)+\mu\gamma}, \qquad \Phi_1 = \mu+\alpha+u_2, \qquad \Phi_2 = \delta+\mu+u_3.$$

To determine whether the controls κ_1 and κ_2 can mitigate measles, it is necessary to examine whether the controls can reduce R_0. The derivatives of R_0 in (3.2), with respect to κ_1 and κ_2 are given by

$$\frac{\partial R_0}{\partial \kappa_1} = -\frac{\beta S_0}{(\Phi_1 + \kappa_1)^2}\left[1 + \frac{\alpha}{\Phi_2 + \kappa_2}\right], \qquad \frac{\partial R_0}{\partial \kappa_2} = -\frac{\alpha\beta S_0}{(\Phi_2 + \kappa_1)^2}.$$

It is clear that $\frac{\partial R_0}{\partial \kappa_1} < 0$ and $\frac{\partial R_0}{\partial \kappa_2} < 0$. This means that both controls κ_1 and κ_2 can reduce the measles.

3.2. Nonlinear Robust Sliding Mode Control Design

3.2.1 Nonlinear sliding mode control law

The design of nonlinear robust sliding mode control is presented in this section. The aim of the control design is to drive the exposed (E) and infected (I) compartments to zero, that is $E(t) \to 0$ and $I(t) \to 0$ as $t \to \infty$, in the presence of parameter uncertainties of the model (3.1). This is achieved by tracking specified decreasing reference signals ($E_{ref} \to 0$ and $I_{ref} \to 0$), employing treatments κ_1 for exposed (E) individuals and κ_2 for infected (I) individuals. To proceed, define the tracking errors at time t as

$$\tilde{E}(t) = E(t) - E_{ref}(t), \qquad \tilde{I}(t) = I(t) - I_{ref}(t), \tag{3.3}$$

where $E_{ref}(t)$ and $I_{ref}(t)$ are the tracking reference signals satisfying

$$\begin{aligned} E_{ref}(0) = E(0), \qquad I_{ref}(0) = I(0), \\ E_{ref}(t) \to 0, \qquad I_{ref}(t) \to 0, \ \ t \to \infty. \end{aligned} \tag{3.4}$$

Equation (3.4) implies that the tracking errors are initially zero, i.e. $\tilde{E}(0) = 0 =$ and $\tilde{I}(0) = 0$, and that the reference signals, E_{ref} and I_{ref}, converge to zero. The control design aims to ensure that the tracking errors, $\tilde{E}$ and $\tilde{I}$, stay or asymptotically converge to zero for all time t despite the uncertainties in the model parameters, thereby implicatively driving the E and I compartments to zero. The reference signals can be formulated to satisfy (3.4) and are hence proposed to be

$$\begin{aligned} E_{ref}(t) &= \left(E(0) - E_{ref}(tf)\right)e^{-\zeta t} + E_{ref}(tf), \\ I_{ref}(t) &= \left(I(0) - I_{ref}(tf)\right)e^{-\zeta t} + I_{ref}(tf), \end{aligned} \tag{3.5}$$

where ζ is a positive constant determining the rate at which the reference signal converges to zero. Then, define sliding functions as

$$s_E(t) = \tilde{E}(t), \qquad s_I(t) = \tilde{I}(t). \tag{3.6}$$

The derivatives of the sliding functions are

$$\begin{aligned} \dot{s}_E(t) &= \dot{\tilde{E}}(t) = \beta S(E + I) - (\mu + \alpha + u_2)E - \kappa_1 E + \zeta\left(E(0) - E_{ref}(tf)\right)e^{-\zeta t}, \\ \dot{s}_I(t) &= \dot{\tilde{I}}(t) = \alpha E - (\delta + \mu + u_3)I - \kappa_2 I + \zeta\left(I(0) - I_{ref}(tf)\right)e^{-\zeta t}. \end{aligned} \tag{3.7}$$

To ascertain that the control objective is attained, the sliding surfaces are defined as

$$s_E(t) = \tilde{E}(t) = 0, \qquad s_I(t) = \tilde{I}(t) = 0. \tag{3.8}$$

Now, the process of designing sliding mode control involves two steps: first, determining the equivalent control κ_{eq} to maintain the system on the sliding surface, and second, determining the switching control κ_{sw} to force the system to slide in the sliding surface [13]. To obtain the equivalent controls, take the derivatives of (3.8) with respect to time t, i.e.

$$\dot{s}_E(t) = 0, \qquad \dot{s}_I(t) = 0. \tag{3.9}$$

Solving equation (3.9) for $\kappa_1(t)$ and $\kappa_2(t)$ yields the following equivalent controls.

$$\begin{aligned} \kappa_{1,eq}(t) &= \frac{1}{E}\left[\beta S(t)\big(E(t)+I(t)\big) - (\mu+\alpha+u_2)E(t) + \zeta\left(E(0) - E_{ref}(tf)\right)e^{-\zeta t}\right], \\ \kappa_{2,eq}(t) &= \frac{1}{I}\left[\alpha E(t) - (\delta+\mu+u_3)I(t) + \zeta\left(I(0) - I_{ref}(tf)\right)e^{-\zeta t}\right]. \end{aligned} \tag{3.10}$$

As the parameters of the system (3.1) contain uncertainties, the estimations of the corresponding parameters are used. For practicality, write

$$\begin{aligned} a &= \beta S(t)\big(E(t)+I(t)\big), & \hat{a} &= \hat{\beta} S(t)\big(E(t)+I(t)\big), \\ b &= \mu+\alpha+u_2, & \hat{b} &= \hat{\mu}+\hat{\alpha}+\hat{u}_2, \\ c &= \delta+\mu+u_3, & \hat{c} &= \hat{\delta}+\hat{\mu}+\hat{u}_3, \end{aligned}$$

and the resulting equivalent controls are

$$\begin{aligned} \kappa_{1,eq}(t) &= \frac{1}{E}\left[\hat{a} - \hat{b}E(t) + \zeta\left(E(0) - E_{ref}(tf)\right)e^{-\zeta t}\right], \\ \kappa_{2,eq}(t) &= \frac{1}{I}\left[\hat{\alpha}E(t) - \hat{c}I(t) + \zeta\left(I(0) - I_{ref}(tf)\right)e^{-\zeta t}\right], \end{aligned} \tag{3.11}$$

where $\hat{\beta}, \hat{\alpha}, \hat{\mu}, \hat{\delta}, \hat{u}_2$, and $\hat{u}_3$ are the estimated values which lie within a bounded error range relative to the actual parameters. To achieve the control objective despite the difference between the actual and estimated values of the parameters in the system (3.1), the following switching controls are required.

$$\kappa_{1,sw}(t) = \frac{g_1(x,t)}{E(t)}\operatorname{sgn}\big(s_E(t)\big), \qquad \kappa_{2,sw}(t) = \frac{g_2(x,t)}{I(t)}\operatorname{sgn}\big(s_I(t)\big), \tag{3.12}$$

where sgn is the sign function and $g_1(x,t), g_2(x,t)$ are switching gains updated through adaptation process to handle the model uncertainties. The switching controls (3.12) need to be augmented to the equivalent controls (3.11), yielding the robust sliding mode control:

$$\begin{aligned} \kappa_1(t) &= \kappa_{1,eq}(t) + \frac{g_1(x,t)}{E(t)}\operatorname{sgn}\big(s_E(t)\big), \\ \kappa_2(t) &= \kappa_{2,eq}(t) + \frac{g_2(x,t)}{I(t)}\operatorname{sgn}\big(s_I(t)\big), \end{aligned} \tag{3.13}$$

where $\kappa_{1,eq}(t)$ and $\kappa_{2,eq}(t)$ are given in (3.11). The switching gains in the resulting controls (3.13) is to be determined to guarantee the convergence of the tracking errors (3.3) to zero.

3.2.2. Adaptation of Switching Gains and Lyapunov Stability

This section presents the stability of the closed-loop system and the tracking error convergence to zero. In order to guarantee the robustness of the controls (3.13) in achieving tracking objectives against parameter uncertainties, the following assumptions are required.

Assumption 1. There exist positive state-dependent functions $\rho_1(x,t)$ and $\rho_2(x,t)$ such that

$$\begin{aligned} \left|(a-\hat{a})-\left(b-\hat{b}\right)E(t)\right| &\leq \rho_1(x,t), \\ |(\alpha-\hat{\alpha})E(t)-(c-\hat{c})I(t)| &\leq \rho_2(x,t), \end{aligned} \tag{3.14}$$

hold for all $t \geq 0$.

The functions $\rho_1(x,t)$ and $\rho_2(x,t)$ always exist, as the system (3.1) is characterised by specific yet unknown parameter values. Epidemiologically, Assumption 1 can be restated as

$$\begin{aligned} \left|(a-\hat{a})-\left(b-\hat{b}\right)E(t)\right| = E(t)\left|\kappa_{true_{1,eq}}-\kappa_{1,eq}\right| &\leq \rho_1(x,t), \\ |(\alpha-\hat{\alpha})E(t)-(c-\hat{c})I(t)| = I(t)\left|\kappa_{true_{2,eq}}-\kappa_{2,eq}\right| &\leq \rho_2(x,t), \end{aligned} \tag{3.15}$$

where $\kappa_{true_{1,eq}}(t)$, $\kappa_{true_{2,eq}}(t)$ are the equivalent controls with actual parameter values and $\kappa_{1,eq}(t)$, $\kappa_{2,eq}(t)$ are the equivalent controls with estimated parameter values. In other words, Assumption 1 implies that the errors caused by parameters mismatches in treatment interventions for exposed (E) and infected (I) individuals are bounded by certain functions.

Assumption 2. The functions $\rho_1(x,t)$ and $\rho_2(x,t)$ are known.

Later on, Assumption 2 will be relaxed as the switching gains are updated through the adaptation process. This process does not require any prior knowledge of model parameters or their bounds.

Assumption 3. The switching gains, $g_1(x,t)$ and $g_2(x,t)$, are defined as

$$\begin{aligned} g_1(x,t) &= \rho_1(x,t)+\varrho_1, \\ g_2(x,t) &= \rho_2(x,t)+\varrho_2, \end{aligned} \tag{3.16}$$

where $\varrho_1, \varrho_2 > 0$. Further, it is assumed that there exist finite positive constants, $\bar{\rho}_1$ and $\bar{\rho}_2$, such that

$$\rho_1(x,t) \leq \bar{\rho}_1, \qquad \rho_2(x,t) \leq \bar{\rho}_2,$$

for all $t \geq 0$. Hence, $g_1(x,t)$ and $g_2(x,t)$ are bounded.

Up to this point, it has been observed that the upper limits, $\rho_1(x,t)$ and $\rho_2(x,t)$, of the discrepancies caused by parameter uncertainties are necessary to calculate the switching gains $g_1(x,t)$ and $g_2(x,t)$. Therefore, to eliminate the need for prior knowledge of these upper bounds, the switching gains will be updated automatically online by

$$\begin{aligned}\frac{d\hat{g}_1(t)}{dt} &= \Upsilon_E s_E(t)\mathrm{sgn}\big(s_E(t)\big),\\ \frac{d\hat{g}_2(t)}{dt} &= \Upsilon_I s_I(t)\mathrm{sgn}\big(s_I(t)\big),\end{aligned} \tag{3.17}$$

where $\hat{g}_1(0) = 0$, $\hat{g}_2(0) = 0$, and Υ_E, Υ_I are positive constants set by the designer. Υ_E and Υ_I determine the rate of switching gain updating with respect to tracking errors, $\tilde{E}$ and $\tilde{I}$. Now, the nonlinear sliding mode controls become

$$\begin{aligned}\kappa_1(t) &= \kappa_{1,eq}(t) + \frac{\hat{g}_1(x,t)}{E(t)}\mathrm{sgn}\big(s_E(t)\big),\\ \kappa_2(t) &= \kappa_{2,eq}(t) + \frac{\hat{g}_2(x,t)}{I(t)}\mathrm{sgn}\big(s_I(t)\big),\end{aligned} \tag{3.18}$$

where $\kappa_{1,eq}(t)$ and $\kappa_{2,eq}(t)$ are given in (3.11).

Based on these assumptions, the following theorem establishes the convergence of tracking errors to zero and its robustness against parameter uncertainties.

Theorem 3.1. *Consider the measles model (3.1) with the sliding mode controls (3.18). If Assumptions 1, 2, and 3 hold, then the tracking errors (3.3) vanish asymptotically.*

Proof. As Assumption 3 holds, there exists finite positive constants $\bar{g}_1$ and $\bar{g}_2$ such that $\bar{\rho}_1 + \varrho_1 \leq \bar{g}_1$ and $\bar{\rho}_2 + \varrho_2 \leq \bar{g}_2$, for any $\varrho_1, \varrho_2 > 0$. Define Lyapunov function as

$$V(t) = \frac{1}{2}\left[s_E^2(t) + s_I^2(t) + \frac{1}{\Upsilon_E}\tilde{g}_1(t)^2 + \frac{1}{\Upsilon_I}\tilde{g}_2(t)^2\right], \tag{3.19}$$

where $\tilde{g}_1(t) = \hat{g}_1(t) - \bar{g}_1$ and $\tilde{g}_2(t) = \hat{g}_2(t) - \bar{g}_2$. Its time-derivative is given by

$$\begin{aligned}\dot{V}(t) &= s_E(t)\dot{s}_E(t) + s_I(t)\dot{s}_I(t)(t) + \frac{1}{\Upsilon_E}\tilde{g}_1(t)\dot{\tilde{g}}_1(t) + \frac{1}{\Upsilon_I}\tilde{g}_2(t)\dot{\tilde{g}}_2(t)\\ &= s_E(t)\big[(a-\hat{a}) - \big(b-\hat{b}\big)E(t) - \hat{g}_1(x,t)sgn\big(s_E(t)\big)\big]\\ &\quad + s_I(t)\big[(\alpha-\hat{\alpha})E(t) - (c-\hat{c})I(t) - \hat{g}_2(x,t)sgn\big(s_I(t)\big)\big] + (\hat{g}_1(t) - \bar{g}_1)|s_E(t)|\\ &\quad + (\hat{g}_2(t) - \bar{g}_2)|s_I(t)|\end{aligned} \tag{3.20}$$

By using Assumptions 1, 2, and 3, it is proved that

$$\begin{aligned}\dot{V}(t) &\leq \rho_1(x,t)s_E(t) - \hat{g}_1(x,t)|s_E(t)| + \rho_2(x,t)s_I(t) - \hat{g}_2(x,t)|s_I(t)|\\ &\qquad + (\hat{g}_1(t) - \bar{g}_1)|s_E(t)| + (\hat{g}_2(t) - \bar{g}_2)|s_I(t)|\\ &= \rho_1(x,t)s_E(t) + \rho_2(x,t)s_I(t) - \bar{g}_1|s_E(t)| - \bar{g}_2|s_I(t)|\\ &\leq \rho_1(x,t)|s_E(t)| + \rho_2(x,t)|s_I(t)| - \bar{\rho}_1|s_E(t)| - \varrho_1|s_E(t)| - \bar{\rho}_2|s_I(t)| - \varrho_2|s_I(t)|\\ &\leq -\varrho_1|s_E(t)| - \varrho_2|s_I(t)| \leq 0.\end{aligned} \tag{3.21}$$

Therefore, the Lyapunov function (3.19) is clearly positive definite and radially unbounded, whereas its derivative, $\dot{V}(t)$, is negative semidefinite. According to Lyapunov stability theorem [11], the origin, $\big(s_E(t), s_I(t)\big) = (0,0)$, is globally stable. In order to show that the origin is asymptotically stable, the Barbalat's Lemma is employed [11].

Now, define $w(t) = \varrho_1|s_E(t)| + \varrho_2|s_I(t)|$. Clearly, function w is uniformly continuous. Further, the inequality (3.21) can be reformulated as

$$\dot{V}(t) \leq -\varrho_1|s_E(t)| - \varrho_2|s_I(t)| = -w(t).$$

Hence,

$$\lim_{t\to\infty} \int_0^t w(\tau)d\tau \leq V(0) - \lim_{t\to\infty} \int_0^t V(\tau)d\tau$$

Since $V(t)$ is positive definite and $\dot{V}(t) \leq 0$, then $V(0) - \lim_{t\to\infty} \int_0^t V(\tau)d\tau$ is positive and finite. This implies that $\lim_{t\to\infty} \int_0^t w(\tau)d\tau$ exists and finite. Hence, based on the Barbalat's lemma [11],

$$\lim_{t\to\infty} w(t) = \lim_{t\to\infty} \varrho_1|s_E(t)| + \varrho_2|s_I(t)| = \lim_{t\to\infty} \varrho_1\left|\tilde{E}(t)\right| + \varrho_2\left|\tilde{I}(t)\right| = 0.$$

As $\varrho_1, \varrho_2 \geq 0$, then it is proved that the tracking errors, $\tilde{E}$ and $\tilde{I}$, converge to zero as $t \to \infty$. ■

Thus, it was proven that the proposed nonlinear robust sliding mode controls (3.18) ensures that the tracking errors (3.3) converge to zero, despite the parameter uncertainties of the system (3.1). Hence, the tracking objective of driving the exposed (E) and infected (I) compartments to zero is achieved. However, it should be noted that the controls (3.18) may exhibit singularities when $E = 0$ and $I = 0$. Nevertheless, Theorem 3.1 states that the asymptotic stability of the tracking errors (3.3) implies that the E and I compartments will not become exactly zero but rather remain positive, yet small, as desired. Conversely, if the the E and I compartments become exactly zero, the corresponding controls κ_1 and κ_2 are undefined and can be considered as zero. This means that the treatments κ_1 and κ_2 are not needed when the number of exposed (E) and infected (I) individuals are already zero, which is epidemiologically valid.

3.3. Numerical Simulations and Discussions

Numerical simulations are presented in this section to evaluate the effectiveness of the resulting nonlinear robust sliding mode controls in eliminating measles against parameter uncertainties. With regard to this, the assumed actual parameter values of the model (3.1) are given in Table 3.1, with initial values of the states are $S(0) = 700$, $V(0) = 400$, $E(0) = 250$, $I(0) = 50$, and $R(0) = 0$. The simulations are performed for 8 years. The nonlinear robust sliding mode controls (3.18) are proposed to drive the exposed (E) dan infected (I) compartments to zero at the end of simulations by tracking the reference signals, respectively E_{ref} and I_{ref}, given in (3.5). For simplicity, the updating rates of switching gains in (3.17) are considered to be $\Upsilon_E = \Upsilon_I = \Upsilon = 3$, and $\zeta = 0.5$. It should be noted that all simulations are conducted numerically, with no fitting to empirical data.

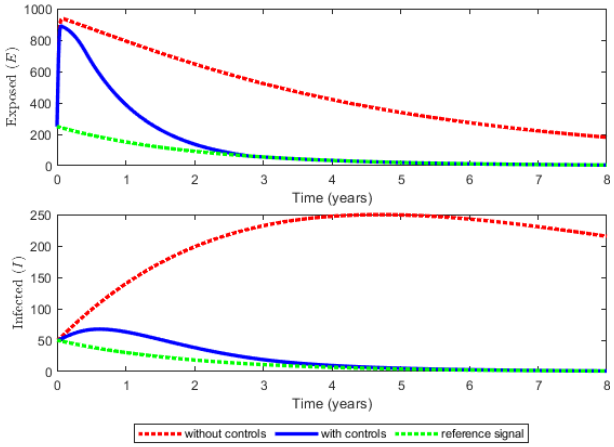

Figure 3.1. Dynamics of the exposed (E) and infected (I) compartments, given a 50% uncertainty.

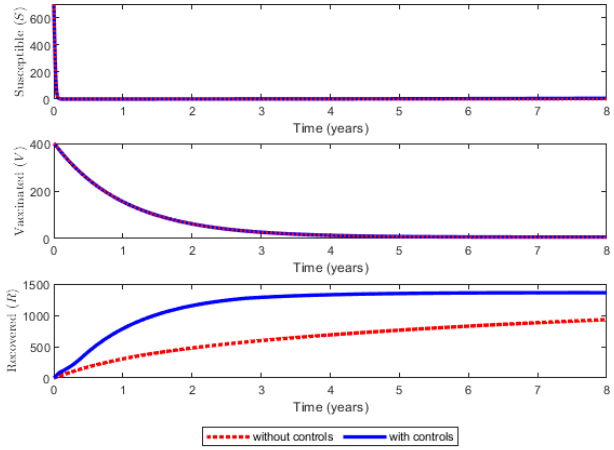

Figure 3.2. Dynamics of the susceptible (S), vaccinated (V), and recovered (R) compartments, given a 50% uncertainty.

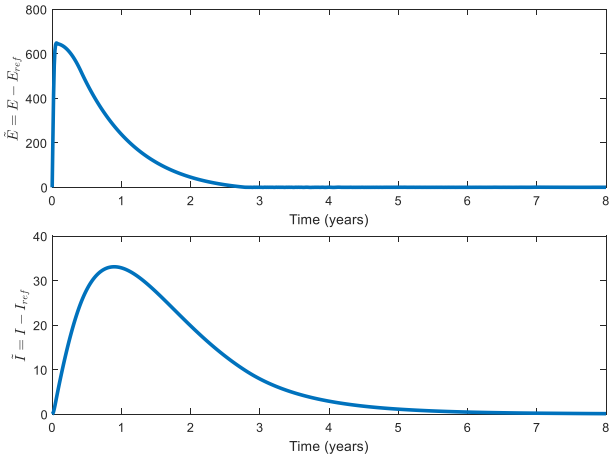

Figure 3.3. Tracking errors, given a 50% uncertainty.

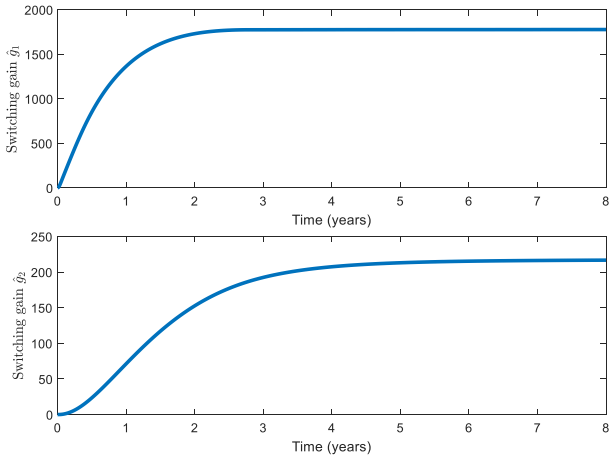

Figure 3.4. Adaptation process of switching gains (3.17), given a 50% uncertainty.

In the presence of 50% uncertainty, the controlled dynamics of measles are presented in Figures 3.1 and 3.2. It is shown that the tracking objective of reducing the number of exposed (E) and infected (I) individuals are achieved. It is in accordance with the tracking errors $\tilde{E}$ and $\tilde{I}$ converging to zero, respectively, after 3.5 years and 6.5 years, as shown in Figure 3.3. Further, Figure 3.4 shows the adaptation processes of switching gains $\hat{g}_1$ dan $\hat{g}_2$ that reach their steady-state values after reaching the sliding condition, that is $\tilde{E} = 0$ and $\tilde{I} = 0$. Besides, as the tracking objective is achieved, Figure 3.2 shows that the populations become immune or progress to the recovered (R) compartment, leaving susceptible (S) dan vaccinated (V) individuals to diminish. The implemented sliding mode controls reduce the number of exposed (E) and infected (I) individuals, respectively, by 80,99% and 84,41%, on average. The control profiles required to meet the tracking objectives are given in Figure 3.5. It should be noted that the treatment controls for exposed (E) and infected (I) individuals, κ_1 and κ_2, respectively, should be within $[0,0.9]$. Figure 3.5 shows that the treatment for infected individuals (κ_2) is fixed at its maximum value, 0.9, throughout the simulation. Meanwhile, the treatment for exposed individuals (κ_1) starts at its maximum before dropping to zero. It gradually starts increasing to its maximum in the first year and remains at that value until 2.8 years. This implies that the first interventions must be implemented to the fullest extent possible in order to eradicate the disease. However, the value of κ_1 switches between zero and its maximum from the 2.8th to 6.7th year. The switching on/off of this control input is called the *chattering* phenomenon.

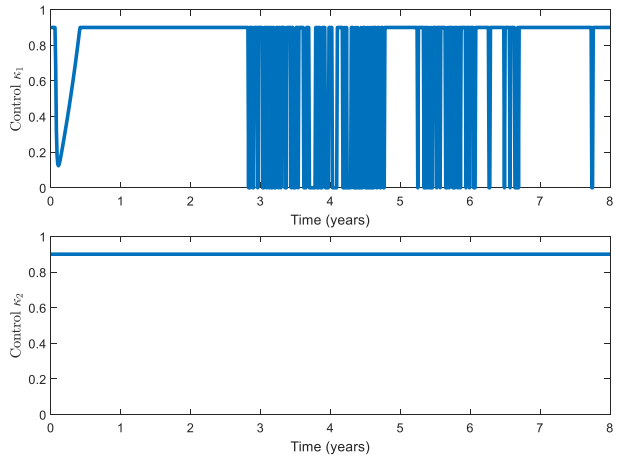

Figure 3.5. Control profiles, given a 50% uncertainty.

3.3.1. Chattering Incidents and Convergence Rates of Tracking Errors

The chattering phenomenon arises as the oscillations of the system output or applied control with finite amplitude and frequency. The chattering phenomenon usually happens during the implementation of sliding mode control, caused by unmodeled dynamics or discontinuity in the system [12]. The chattering of the control input κ_1, as shown in Figure 3.5, makes its implementation difficult. In this case, the chattering is caused by the discontinuity of the "sgn" function in the controllers (3.18). Hence, to reduce the chattering, approximate continuous differentiable functions, such as saturation or tangent hyperbolic function, can be used instead of the "sgn" function [9, 14]. Here, we use the tangent hyperbolic functions: $\tanh(0.01\tilde{E})$ and $\tanh(0.01\tilde{I})$, also saturation functions: $\mathrm{sat}(\tilde{E})$ and $\mathrm{sat}(\tilde{I})$, defined in [9] as

$$\mathrm{sat}(x) = \begin{cases} \mathrm{sgn}(x) & \text{if } |x| > \Psi \\ \dfrac{x}{\Psi} & \text{if } |x| < \Psi' \end{cases}$$

where $\Psi > 0$ is constant, as alternatives to $\mathrm{sgn}(\tilde{E})$ and $\mathrm{sgn}(\tilde{I})$, respectively. Figure 3.6 shows that controllers with three functions have similar tracking errors which diminish to zero by the end of the simulations. Nevertheless, the tracking error $\tilde{I}$ for the sat and tanh functions are converging more slowly than those for the sgn function. This is indicated by the minimum time needed for the tracking error $\tilde{I}$ to be less than 0.5, which is longer for the sat and tanh functions (6.82 and 6.96 years, respectively) than for the sign function (5.92 years). This is in accordance with the control κ_2 for the sat and tanh functions, which are not employed at their maximum value throughout the simulation, see Figure 3.7. Besides, the alternative functions, sat and tanh, produce much smoother controls, especially κ_1, compared to when the sgn function is used.

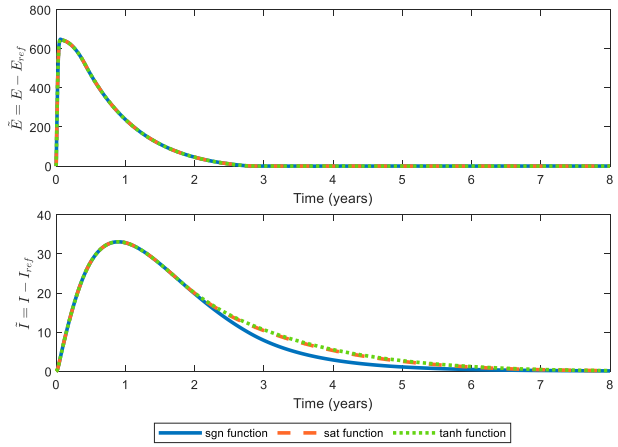

Figure 3.6. Tracking errors for three different functions in the controllers (3.18), given a 50% uncertainty.

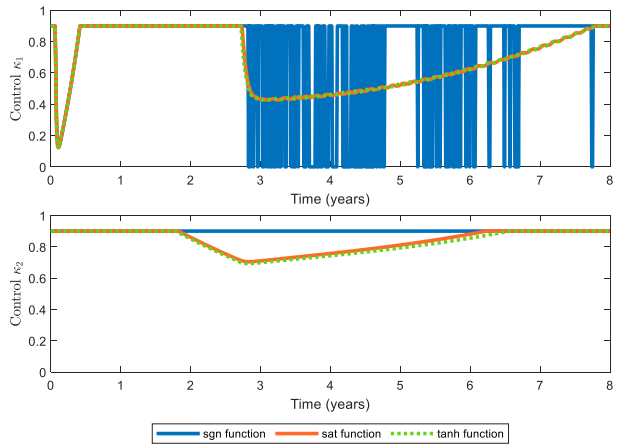

Figure 3.7. Control profiles for three different functions in the controllers (3.18), given a 50% uncertainty.

According to [12], the magnitude of the control does affect how intense the chattering is. Figure 3.8 shows that, with the sgn function in the controllers (3.18), the control κ_1 switches on and off over a longer time interval as the value of Υ in switching gain adaptation (3.17), increases, as further justified by the Table 3.2. This is in accordance with the amplitude of the switching gains $\hat{g}_1$ and $\hat{g}_2$, shown in Figure 3.9, which are bigger as the value of Υ increases. Even in the case where Υ is 0.1, there is no chattering. This implies that the intensity of the chattering is proportional to the sizes of the switching gains, as in [12]. Besides, the control κ_1 increases to its maximum value earlier after dropping down at the start, as Υ increases. Figure 3.10 shows that the rates at which the tracking errors, $\tilde{E}$ and $\tilde{I}$, converge to zero, accelerate as Υ increases. It is also observed that it takes longer for tracking errors to converge to zero for smaller values of Υ, particularly when $\Upsilon = 0.1$. The minimum times needed for the tracking errors $\tilde{E}$ and $\tilde{I}$ to be less than 0.5 for different values of Υ are given in Table 3.2. This implies that the chattering of control κ_1 intensifies to achieve faster convergence rates to the desired reference signals, while the control κ_2 remains at its maximum value throughout the simulation. On the other hand, Table 3.2 also suggests that the

larger the values of Υ, the greater the reduction average of the number of exposed (E) and infected (I) individuals.

Table 3.2. Quantitative measures of control performance for different values of Υ

Υ	Reduction Average (%)		Minimum time (years) for tracking error < 0.5		Estimated length of control κ_1 chattering interval
	E	I	$\tilde{E}$	$\tilde{I}$	
5	81.89	84.91	2.65	5.81	4.11
3	80.99	84.42	2.78	5.92	3.86
1	76.85	82.44	3.4	6.39	3.27
0.1	40.59	73.14	>8	>8	0

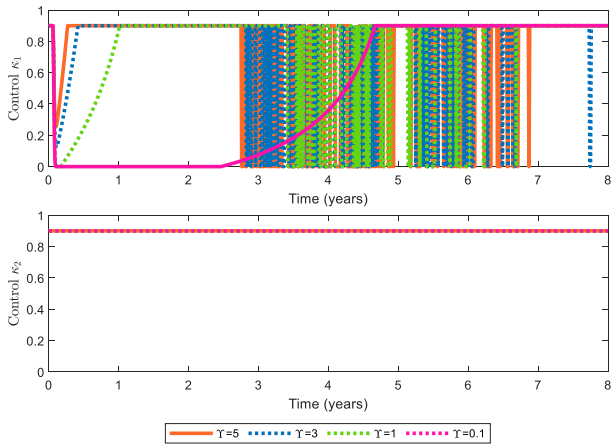

Figure 3.8. Control profiles for different values of Υ in the adaptation process of switching gains (3.17), given a 50% uncertainty.

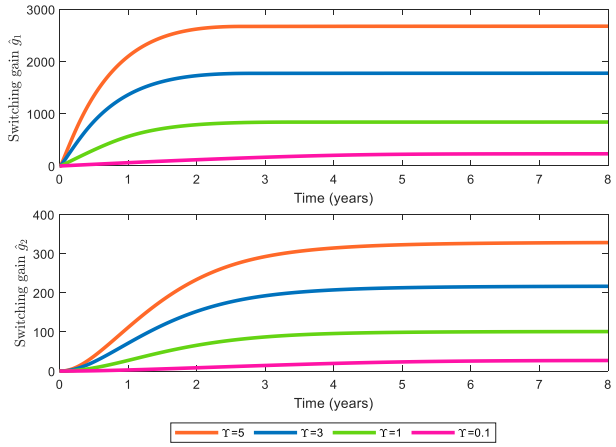

Figure 3.9. Adaptation process of switching gains (3.17) for different values of Υ, given a 50% uncertainty.

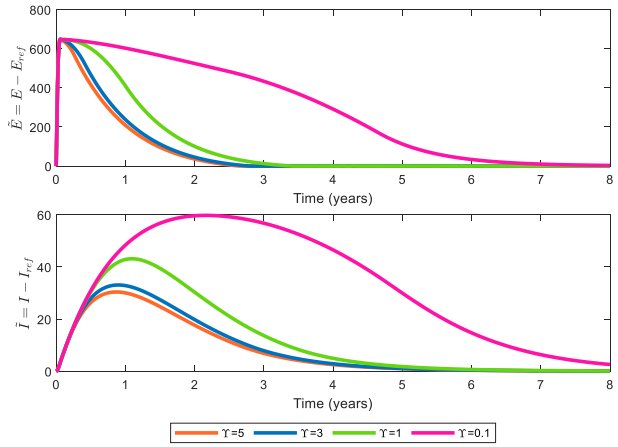

Figure 3.10. Tracking errors for different values of ϒ in the adaptation process of switching gains (17), given a 50% uncertainty.

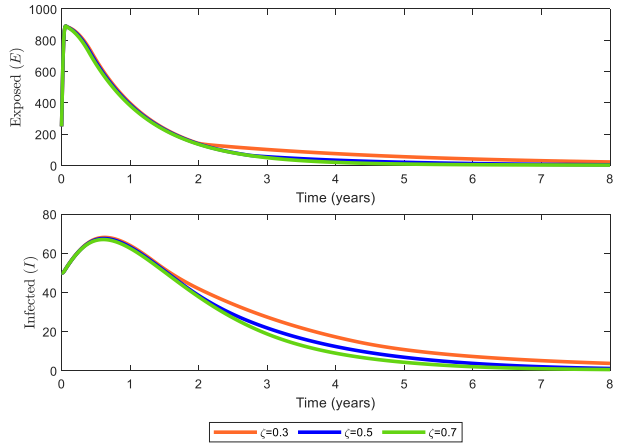

Figure 3.11. Dynamics of the exposed (E) and infected (I) compartments for different values of ζ in the reference signals, with tanh function in the controllers (3.18) given a 50% uncertainty.

Table 3.3. Quantitative measures of control performance for different values of ζ

ϒ	Reduction Average (%)		Minimum time (years) for tracking error < 0.5	
	E	I	$\tilde{E}$	$\tilde{I}$
0.3	73.71	82.54	2.57	4.51
0.5	81.02	83.98	2.83	6.96
0.7	82.81	84.72	>8	7.38

On the other hand, the decreasing rates of E and I trajectories to zero is affected by ζ in the reference signals E_{ref} and I_{ref}, respectively, and hence in the controllers (3.18). As can be seen in Figure 3.11, the trajectories of E and I decrease to zero faster as the value of ζ increases. It is followed by the larger reduction averages of the number of exposed (E) and infected (I) individuals as the value of ζ increases, as shown in Table 3.3. However, this does not mean that the convergence rates to zero of tracking errors, $\tilde{E}$ and $\tilde{I}$, are also faster, as displayed in Figure 3.12. Table 3.3 further

explains that the minimum times required for the tracking errors $\tilde{E}$ and $\tilde{I}$ to be less than 0.5 is longer for the larger values of ζ. The more rapid decline to zero of E and I trajectories is accomplished by the lengthier interval during which the control κ_1 and κ_2 are at maximum, as shown in Figure 3.13. This is epidemiologically valid, as the maximum interventions need to be implemented for longer if the disease is to be eradicated quickly.

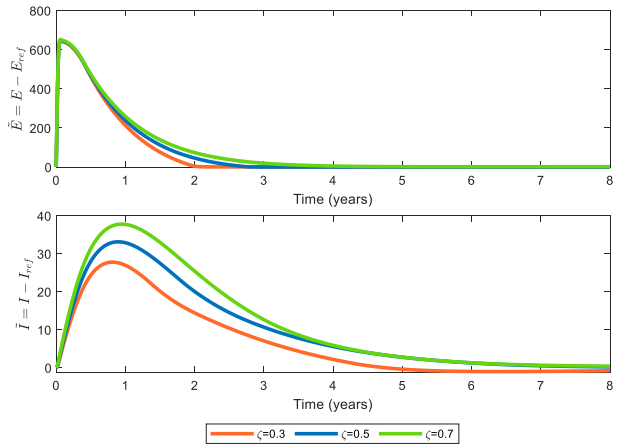

Figure 3.12. Tracking errors for different values of ζ in the reference signals, with tanh function in the controllers (3.18) given a 50% uncertainty.

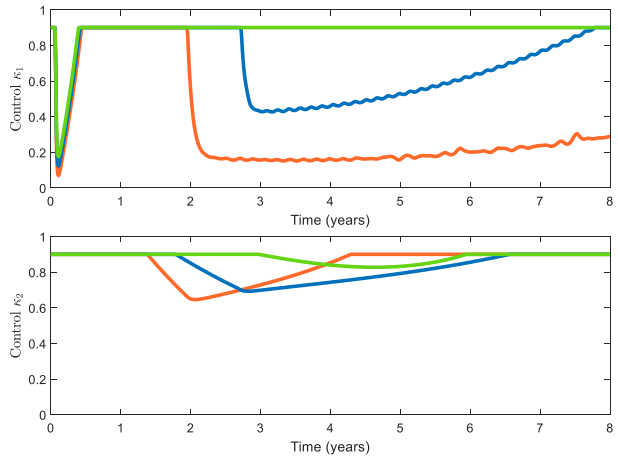

Figure 3.13. Control profiles for different values of ζ in the reference signals, with tanh function in the controllers (3.18) given a 50% uncertainty.

3.3.2. Parameter Uncertainties

The dynamics of measles (3.1) may contain uncertainties in their parameter values. This is caused by factors affecting the spread of measles for different populations, environments, and demographics, which may be different. How parameter uncertainties affect the performance of nonlinear robust sliding mode controls (3.18) in diminishing the numbers of exposed (E) and infected (I) individuals will be evaluated. Here, we consider different cases of how uncertainties are distributed among the estimated parameters $\hat{\beta}$, $\hat{\mu}$, $\hat{\alpha}$, $\hat{\delta}$, $\hat{u}_2$, and $\hat{u}_3$ in the controllers (3.18), as shown in Table 3.4. The levels of uncertainty being considered are $\pm 30\%$, $\pm 50\%$, and $\pm 80\%$. It should be noted that more than 50% uncertainty is only theoretical and may not possible in real

situations. The value of corresponding estimated parameter $\hat{\theta}$ with the level of uncertainty Δ is $\hat{\theta} = (1 + 0.01\Delta) \cdot \theta$, where θ is the assumed actual parameter. The tracking errors $\tilde{E}$ and $\tilde{I}$ for eight different cases with the tanh function in the controllers (3.18), are shown in Figure 3.14.

Table 3.4. Different cases of paramater uncertainties

	Percentage of uncertainty (Δ%)					
Cases	$\hat{\beta}$	$\hat{\mu}$	$\hat{\alpha}$	$\hat{\delta}$	$\hat{u}_2$	$\hat{u}_3$
1.	+80	+80	+80	+80	+80	+80
2.	+50	+50	+50	+50	+50	+50
3.	+30	+30	+30	+30	+30	+30
4.	+80	-50	+30	-30	-80	+50
5.	-30	-80	-50	+50	+80	+30
6.	-30	-30	-30	-30	-30	-30
7.	-50	-50	-50	-50	-50	-50
8.	-80	-80	-80	-80	-80	-80

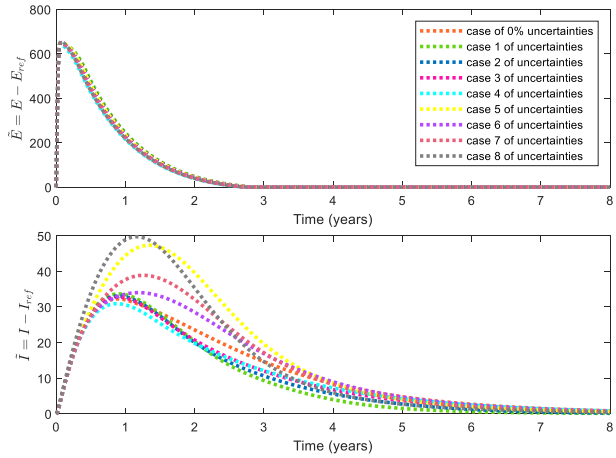

Figure 3.14. Tracking errors for different cases of parameter uncertainties, with tanh function in the controllers (3.18).

Different cases of parameter uncertainties will lead to a different measles outbreak, especially the peaks of the exposed (E) and infected (I) compartments. The robustness of the sliding mode controllers (3.18) will therefore be required to handle the uncertainties. Figure 3.14 shows that the tracking errors for different cases of parameter uncertainties show similar dynamics but different values in the beginning, and steadily converge towards zero. The minimum times required for the tracking errors $\tilde{E}$ to be less than 0.5 are shown to be in the range of 2.69–2.86 years, and at least 6.17 years for $\tilde{I}$, as demonstrated in Table 3.5. Besides, the controls κ_1 and κ_2 needed to track the reference signals are adjusted, as shown in Figure 3.15. Employing this control strategy, both the reduction average in the number of exposed (E) and infected (I) individuals and the RMS of the tracking errors $\tilde{E}$ and $\tilde{I}$ for different cases of parameter uncertainties are not very different, as shown in Table 3.5. This implies that the resulting sliding mode controls perform robustly in decreasing the number of exposed (E) and infected (I) individuals by tracking desired reference signals against parameter uncertainties in the measles model.

Table 3.5. Quantitative measures of control performance for different cases of parameter uncertainties

Case	Reduction Average (%)		Minimum time (years) for tracking error < 0.5		RMS	
	E	I	$\widetilde{E}$	$\widetilde{I}$	$\widetilde{E}$	$\widetilde{I}$
0% uncertainties	81.29	83.23	2.83	>8	170.84	15.78
1	80.82	84.18	2.86	6.17	177.33	14.68
2	81.02	83.98	2.83	6.96	174.65	14.69
3	81.13	83.72	2.85	>8	173.01	14.91
4	81.81	83.86	2.69	>8	164.19	14.31
5	81.09	81.01	2.83	>8	173.46	22.54
6	81.42	82.66	2.76	>8	168.96	17.46
7	81.51	82.22	2.74	>8	167.82	19.04
8	81.57	81.26	2.73	7.81	167.19	22.16

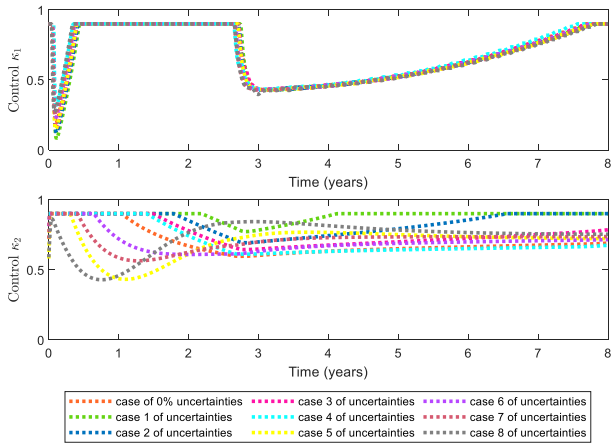

Figure 3.15. Control profiles for different cases of parameter uncertainties, with tanh function in the controllers (3.18).

3. CONCLUSION

In this paper, a nonlinear robust sliding mode control is proposed as a means of eradicating measles by administering treatments to exposed and infected individuals through a desired reference signal tracking scheme while maintaining the existing levels of vaccination. Using Lyapunov's stability theorem and Barbalat's Lemma, it is proven that the proposed sliding mode control achieves the tracking objective despite the model's parameter uncertainties. The performance of the proposed control has been shown to be effective in driving the number of individuals exposed and infected with measles to zero in a number of cases of parameter uncertainties and diminishing rates. The control strategies resulted in the population becoming immune as the susceptible and vaccinated compartments diminished and individuals progressed to the recovered compartment. The simulation results show that maximum intervention should be implemented from the beginning of the outbreak in order to mitigate measles quickly despite uncertainties. However, the dynamics of measles being considered do not take into account the heterogeneity of the population in terms of susceptibility and contact rates, nor the delay effects arising from the latent period and the pre-symptomatic infectious phase of measles. In the future, it would be interesting to incorporate stochastic processes capable of handling population heterogeneity and delay effects, as well as uncertainties arising from limited empirical data, into

the model. This would provide public health authorities with a more accurate insight into mitigation strategies.

ACKNOWLEDGEMENT

This research received no external funding. The authors sincerely thank the editor and reviewers for their insightful comments and suggestions, which greatly improved the quality of this work. Expressions of gratitude are extended to all co-authors for their collaboration, commitment, and valuable contributions to the preparation of this manuscript.

CONFLICT OF INTEREST

The authors declare that there is no conflict of interest

REFERENCES

[1] Ahmad, W., Butt, A. I. K., Rafiq, M., Asif, Z., Ismaeel, T., & Ahmad, N., 2024. Modeling, analyzing and simulating the Measles transmission dynamics through efficient computational optimal control technique. *The European Physical Journal Plus*, *139*(7), 566. https://doi.org/10.1140/epjp/s13360-024-05368-9

[2] Assegaf, F., Saragih, R., & Handayani, D., 2020. Adaptive Sliding Mode Control for Cholera Epidemic Model. *IFAC-PapersOnLine*, *53*(2), 16092–16099. https://doi.org/10.1016/j.ifacol.2020.12.428

[3] Ayu, R. W. S., 2024. Kontrol Sliding Mode Adaptif dengan Vaksinasi dan Treatment pada Model Penyebaran Tuberkulosis. *Epsilon: Jurnal Matematika Murni Dan Terapan*, *18*(1), 54. https://doi.org/10.20527/epsilon.v18i1.12326

[4] Badfar, E., Zaferani, E. J., & Nikoofard, A., 2022. Design a robust sliding mode controller based on the state and parameter estimation for the nonlinear epidemiological model of Covid-19. *Nonlinear Dynamics*, *109*(1), 5–18. https://doi.org/10.1007/s11071-021-07036-4

[5] Berhe, H. W., & Makinde, O. D., 2020. Computational modelling and optimal control of measles epidemic in human population. *Biosystems*, *190*, 104102. https://doi.org/10.1016/j.biosystems.2020.104102

[6] Bhadelia, N., White, L., & Gostin, L., 2025. *The Perfect Storm: Measles Resurgence in an Era of Vaccine Disinformation and the Dismantling of Public Health*. https://doi.org/10.1599/mqop.2025.0410

[7] Chatterjee, A. N., Sharma, S. K., & Al Basir, F., 2024. A Compartmental Approach to Modeling the Measles Disease: A Fractional Order Optimal Control Model. *Fractal and Fractional*, *8*(8), 446. https://doi.org/10.3390/fractalfract8080446

[8] Di Giamberardino, P., & Iacoviello, D. 2019. Analysis, Simulation and Control of a New Measles Epidemic Model. *Proceedings of the 16th International Conference on Informatics in Control, Automation and Robotics*, 550–559. https://doi.org/10.5220/0007934405500559

[9] Ibeas, A., de la Sen, M., & Alonso-Quesada, S., 2014. Robust Sliding Control of SEIR Epidemic Models. *Mathematical Problems in Engineering*, *2014*(1). https://doi.org/10.1155/2014/104764

[10] Jaharuddin, & Bakhtiar, T., 2020. Control Policy Mix in Measles Transmission Dynamics Using Vaccination, Therapy, and Treatment. *International Journal of Mathematics and Mathematical Sciences*, *2020*, 1–20. https://doi.org/10.1155/2020/1561569

[11] Khalil, H. K., 2002. *Nonlinear Systems* (Third Edition). Prentice Hall.

[12] Lee, H., & Utkin, V. I., 2007. Chattering suppression methods in sliding mode control systems. *Annual Reviews in Control*, *31*(2), 179–188. https://doi.org/10.1016/j.arcontrol.2007.08.001

[13] Liu, J., & Wang, X., 2011. *Advanced Sliding Mode Control for Mechanical Systems*. Springer Berlin Heidelberg. https://doi.org/10.1007/978-3-642-20907-9

[14] Sharifi, M., & Moradi, H., 2017. Nonlinear robust adaptive sliding mode control of influenza epidemic in the presence of uncertainty. *Journal of Process Control*, *56*, 48–57. https://doi.org/10.1016/j.jprocont.2017.05.010

[15] van den Driessche, P., & Watmough, J., 2002. Reproduction numbers and sub-threshold endemic equilibria for compartmental models of disease transmission. *Mathematical Biosciences*, *180*(1–2), 29–48. https://doi.org/10.1016/S0025-5564(02)00108-6

[16] Viriyapong, R., & Ridbamroong, W., 2020. Global stability analysis and optimal control of measles model with vaccination and treatment. *Journal of Applied Mathematics and Computing*, *62*(1–2), 207–237. https://doi.org/10.1007/s12190-019-01282-x

[17] World Health Organization, 2024. November 14). *Measles*. https://www.who.int/news-room/fact-sheets/detail/measles

[18] World Health Organization, 2025. *European Region reports highest number of measles cases in more than 25 years – UNICEF, WHO/Europe*. https://www.who.int/europe/news/item/13-03-2025-european-region-reports-highest-number-of-measles-cases-in-more-than-25-years---unicef--who-europe